Computer simulation of core structure and Peierls stress of dislocations in anthracene crystals

1993 J. Phys.: Condens. Matter 5 3151

(http://iopscience.iop.org/0953-8984/5/19/013)

J. Phys.: Condens. Matter 5 (1993) 3151–3162. Printed in the UK

Computer simulation of core structure and Peierls stress of dislocations in anthracene crystals

N Ide†, I Okada‡ and K Kojima‡

† Graduate School of Integrated Science, Yokohama City University, 22–2 Seto, Kanazawa-ku, Yokohama 236, Japan

‡ Department of Physics, Yokohama City University, 22–2 Seto, Kanazawa-ku, Yokohama 236, Japan

Received 2 December 1992, in final form 23 February 1993

Abstract. The equilibrium configuration for the core of a [010] screw dislocation in an anthracene crystal was calculated using the atom–atom potential method. It was strongly anisotropic and complicated due to the characteristic shape and dimension of the molecule. The core region did not spread as much as that of a [010](001) edge dislocation. Its energy was lower than that of the edge dislocation. The Peierls stresses of both the edge and the screw dislocations were estimated by means of gradually increasing an external shear stress; that of the screw dislocation was much larger than that of the edge dislocation.

1. Introduction

It has been recognized through many experimental investigations that dislocations in organic crystals play an important role in solid-state reactions (Cohen *et al* 1969, Williams and Thomas 1972), photoplastic effects (Kojima 1987) and in the formation of local electronic states of polarization origin as well as in mechanical properties (Silinsh 1980, Pertsin and Kitaigorodsky 1987). Investigations into the atomistic structure of the dislocations are essential to understand how the dislocations are concerned with those phenomena. However, numerical calculations for such investigations in molecular solids have been limited in number. A core structure of a dislocation in an organic crystal was first simulated by Mokichev and Pakhomov (1982) for an edge dislocation in a naphthalene crystal. A Peierls stress in organic crystals was first obtained for polyethylene in an orthorhombic phase using computer simulations by Bacon and Tharmalingam (1983). However, for aromatic hydrocarbons, such as anthracene, no calculations of Peierls stresses have yet been carried out. In recent years, with the aid of vector processors, it has become possible to treat a large enough model of crystals composed of large organic molecules.

In anthracene crystals, both (001)[010] slip systems and (001)[110] systems are dominantly operative (Robinson and Scott 1967, Kojima and Okada 1990) and there are also cleavage planes parallel to (001). In a previous paper (Ide *et al* 1990, hereinafter referred to as I), the present authors investigated the equilibrium configuration for the core of a [010](001) edge dislocation in an anthracene crystal using the atom–atom potential method. One problem of particular interest was what structure of the dislocation core was realised in a crystal composed of disk-like molecules possessing a rigid body. The core of the edge dislocation had a spread-out shear misfit along the slip plane, whose width was about $5b$, where b is the magnitude of the Burgers vector. The maximum of compressive strain was only 0.05, even in the core region.

0953-8984/93/193151+12$07.50

On the other hand, the elastic energies of [010] screw dislocations are the lowest of all possible dislocations (Kojima 1979). Therefore the molecular configurations around the [010] screw dislocation is more important than that of the edge dislocations. In addition, the extrapolated yield stresses to 0 K were observed to be $4.6\times10^{-3}\,\mu$ in (001)[010] slip systems by compression experiments (Kojima and Okada 1990), where μ is the shear modulus. It is interesting to know which controls this plastic behaviour, the Peierls stress of screw dislocations or of edge dislocations. Thus both Peierls stresses were estimated by means of increasing an external stress step-by-step until the dislocation moved over the length of a unit lattice vector.

The molecule was assumed to be rigid and the atom–atom potential method was used throughout the present simulations. The magnitude of the radius of the cylindrical region where molecules were movable was taken up to $16b$. In the outer fixed region not only the translational displacements of molecules, on the basis of anisotropic elasticity, but also the rotations of molecules were taken into account with a linear approximation. Both the methods of static energy minimization and of molecular dynamics were used to obtain equilibrium configurations.

2. Core structure of [010] screw dislocations

2.1. Potential and model

We begin with constructing the regular lattice, which is stable under a given potential. The functional form used for the pairwise-additive atom–atom potentials is the Buckingham function, where for empirical parameters we use the values presented by Williams (1966) in set IV (Craig and Markey 1979, Dautant and Bonpunt 1986, Okada *et al* 1989, I). The cut-off radius of interaction between atoms is 8 Å throughout the present simulations. All parameters used in the present simulations, such as elastic constants, are estimated through this potential. The evaluated packing energy and lattice constants (Okada *et al* 1989) agree well with experimental values (Chaplot *et al* 1982), with errors within 2%.

Our model for dealing with the relaxation of molecules around the dislocation consists of two layers. One is the inner cylindrical layer, which consists of the relaxable molecules whose centres lie within a cylinder of radius $r_{\rm rel}$ with its centre at the dislocation line. The other is the outer rigid layer, where molecules are held in the initial configuration. An anisotropic linear elasticity of the dislocation is used in those layers. Translational displacements u using the elasticity can be derived from the general equation given by Hirth and Lothe (1982). Since the anthracene crystal has a glide symmetry with respect to the plane perpendicular to the dislocation line, the displacements u have simple expressions:

$$u_1 = u_3 = 0 \tag{1}$$

$$u_2 = -\frac{b}{2\pi}\tan^{-1}\frac{(c_{44}c_{66}-c_{46}{}^2)^{1/2}x_3}{c_{44}x_1 - c_{46}x_3} \tag{2}$$

where the dislocation line runs along the x_2 axis, and c_{ij} are elastic constants whose values are given in table 1: orthogonal axes x_1, x_2 and x_3 are parallel to the crystallographic axes a, b and c', respectively. In addition to the translational displacements, we introduce molecular rotations into the initial and the boundary conditions to a linear approximation, as we did in I, because anthracene molecules are not small enough, in comparison with the

Table 1. Calculated elastic constants at 0 K and experimental values at room temperature, in unit of GPa.

Calculation		Experiment	
c_{ij}	I	Danno *et al* (1968)	Afanas'eva (1970)
c_{11}	12.40	8.92	8.47
c_{22}	14.53	13.80	11.56
c_{33}	20.13	17.00	14.74
c_{44}	2.85	2.42	2.63
c_{55}	4.58	2.84	2.67
c_{66}	3.39	3.16	3.99
c_{12}	10.42	4.63	7.07
c_{13}	8.40	4.49	5.40
c_{15}	1.38	8.44	4.14
c_{23}	7.52	−2.58	−1.92
c_{25}	1.90	−2.59	−2.38
c_{35}	−5.03	−2.88	−2.14
c_{46}	1.64	1.14	1.40

magnitude of the Burgers vector, to ignore those rotations. To simulate an infinitely long straight dislocation, periodic boundary conditions are imposed along the dislocation line.

To obtain the equilibrium configuration of molecules around the screw dislocation, we have used both the methods of static energy minimization and of molecular dynamics. In static minimization, a method of steepest descent is applied at first, and then a Newton method is used repeatedly until the energies of molecular rows parallel to the dislocation line converge. A line-search method combined with the Newton method was very effective in this simulation for the screw dislocation. In addition to these calculations, for initial states in the static method, we used seven different kinds of molecular configurations obtained in the course of the molecular dynamics calculations at 500 K, so as not to obtain local minimum states. To obtain the equilibrium configuration in the molecular dynamics, the crystal was quenched every time the total kinetic energy reached a maximum (Gibson *et al* 1960). It was confirmed that all these methods gave the same result with errors within 10^{-4}–10^{-6} Å or radian.

Figure 1 shows a projection in the ac plane of a unit cell of a perfect crystal. There are two non-equivalent molecules; one with a centre of mass at crosses in the figure (hereinafter referred to as a corner molecule), the other with a centre of mass at circles in the figure (a centre molecule). The perfect crystal of anthracene has a twofold screw axis parallel to the b axis at the point O. The coordinate of the point O is $\frac{3}{4}a_0 + \frac{1}{2}c_0$, where a_0 and c_0 are unit lattice vectors. The dislocation line is set to run along the b axis.

To search for an adequate position of the dislocation for the initial and boundary conditions, the centre of the dislocation is put at various points along the lines HH′ and VV′ in the figure. The energies after relaxation are compared for these cases using the relaxation radius $r_{rel} = 6b$. When we deal with a right-handed screw dislocation, among the dislocations with centres on the line HH′, that with its centre at the point O had the lowest energy and that with its centre at the point H_1 had the highest energy. For a left-handed screw dislocation, their energies would be replaced. Inequality between the points O and H_1 comes from the fact that the orientation of the corner molecule is different from that of the centre molecules. Among dislocations centred on the line VV′, that with its centre at the point O had the lowest energy. Consequently, the centre of dislocation will be set at the point O in the following simulations.

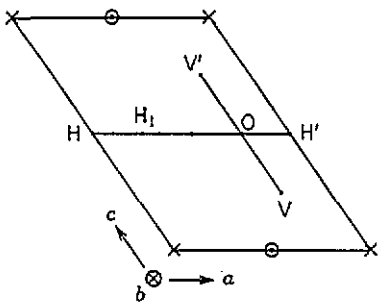

Figure 1. A projection in the *ac* plane of a perfect crystal. Crosses denote the corner molecules and circles denote the centre molecules. The influence on the dislocation energy of changing the position of the dislocation for the boundary condition was evaluated on the lines HH' and VV'.

To evaluate the effects of the model size on molecular configurations, several runs were made using $r_{rel} = 4b$ (24 Å, 48 relaxable molecules) to $16b$ (96 Å, 758 molecules) in the same way as in I. It was confirmed that convergence was much better in the screw dislocation than in the edge dislocation; the differences between molecular coordinates obtained with $r_{rel} = 16b$ and those extrapolated to an infinitely large model were less than 10^{-3} Å or radian. The results of the calculations that will be given in the following subsections were obtained by the use of $16b$ as the relaxation radius r_{rel}.

2.2. *Equilibrium configurations around the dislocation*

Figure 2(*a*) shows a projection in the *ac* plane of molecular centres and a distribution of a shear strain $\varepsilon_{2\theta}$ ($r^{-1}\partial u_2/\partial\theta$, where θ is an angle from the x_1 axis) before the relaxation, and figure 2(*b*) shows those after relaxation. The distribution of the strain $\varepsilon_{2\theta}$ is strongly anisotropic even in an elastic solution. It is due to anisotropy of elastic constants. An elastic constant $c'_{2\theta 2\theta}$ in terms of cylindrical coordinates (r, θ, x_2) is expressed by the elastic constants c_{ij} in terms of cartesian coordinates as follows:

$$c'_{2\theta 2\theta} = A\cos(2\theta + \alpha) + B \tag{3}$$

where

$$A = [\tfrac{1}{4}(c_{44} - c_{66})^2 + c_{46}{}^2]^{1/2} \qquad B = \tfrac{1}{2}(c_{44} + c_{66}) \qquad \alpha = \tan^{-1}\frac{2c_{46}}{c_{44} - c_{66}}.$$

Substitutions of the calculated values for c_{ij} give $A = 1.66$ GPa, $B = 3.12$ GPa and $\alpha = 99.4°$. This elastic constant $c'_{2\theta 2\theta}$ has a minimum value of 1.46 GPa in the direction of $\theta = 40.3°$, and a maximum value of 4.78 GPa in the direction of $\theta = -49.7°$. Since the latter is three times larger than the former, the distribution of the strain $\varepsilon_{2\theta}$ is strongly anisotropic. The direction for the smallest elastic constant is approximately normal to molecular planes and rotations of molecules are easy when a shear stress is applied in that direction.

Figure 2(*b*) shows that the distribution of the shear strain $\varepsilon_{2\theta}$ is hardly influenced by the relaxation on the slip plane AA'. Rotations of molecules around normal axes of molecules contribute to the strain on that plane, so the strain concentrates near the dislocation centre to the same extent as in the elastic solution. The maximum value of the shear strain reaches 0.2

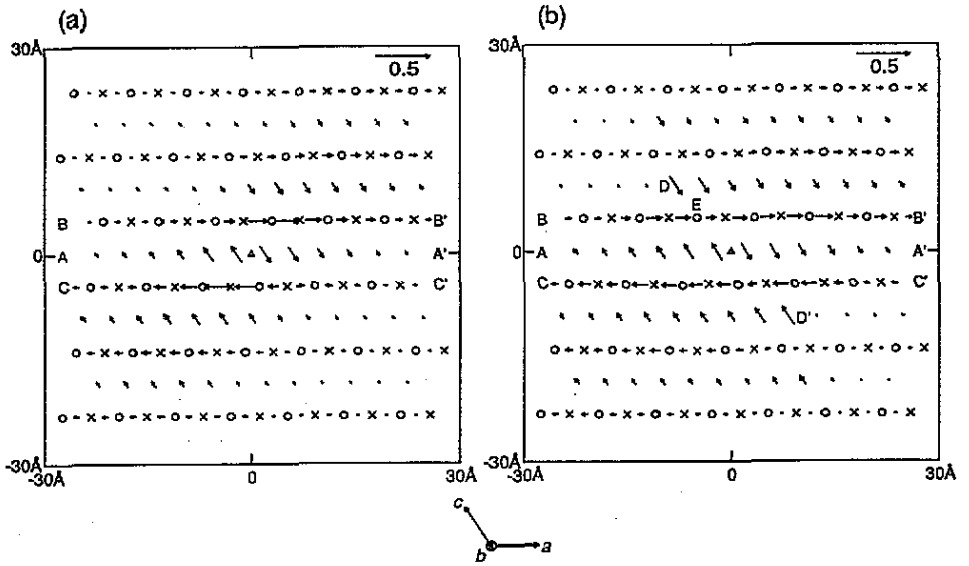

Figure 2. A projection in the *ac* plane of molecular centres around a [010] screw dislocation: (*a*) before the relaxation and (*b*) after the relaxation. A triangle denotes the dislocation centre, crosses the corner molecules, circles the centre molecules. The lengths of arrows indicates the magnitude of the strain $\varepsilon_{2\theta}$. The molecule to which an arrow points is more displaced along positive x_2 direction than the other molecule connected by the arrow.

while, around the edge dislocation simulated in I, that of a compressive strain is only 0.05. On the planes BB′ and CC′, the distribution of the strain spreads out and has two peaks. In these planes, molecules lie close to one another so that the complicated distribution of the strain, which reflects the characteristic shape of anthracene molecules, is realised. The shear strains at the points D and D′ are fairly large, but actual displacements are small because the angles subtended by the dislocation centre are small. The molecular configuration, concerning positions and orientations, has a complete twofold symmetry with respect to the dislocation centre, while that in a perfect crystal has a twofold screw symmetry.

The changes in the Euler angles of the corner molecules on the plane BB′ just above the slip plane are shown in figure 3 (*a*), and those of the centre molecules are shown in figure 3 (*b*). The changes reach maxima near the centre; $\Delta\theta = 6.3°$, $\Delta\phi = 1.2°$ and $\Delta\psi = 14.5°$. This figure shows that the core region does not spread out, in contrast to that of the edge dislocation. The changes in ψ are large and this indicates that the rotations around the normal axes of molecules are the main ones in the core of the screw dislocation.

2.3. Energy distribution

Figure 4 shows equipotential curves ΔE around the dislocation; ΔE is the packing energy per unit lattice cell relative to that of a perfect crystal. Equipotential curves become smooth only if the energies of a corner and centre molecule are summed, because the effects of the shear strains ε_{23} and ε_{12} on the two kinds of molecules are different. The energy distribution spreads a little along the slip plane; far from the centre it spreads in a direction $\theta = 40°$ from the *a* axis. The maximum value of the energy, 0.07 eV, is 0.02 eV smaller than that of the edge dislocation, but the strain of the screw dislocation at the centre is much larger than that of the edge dislocation.

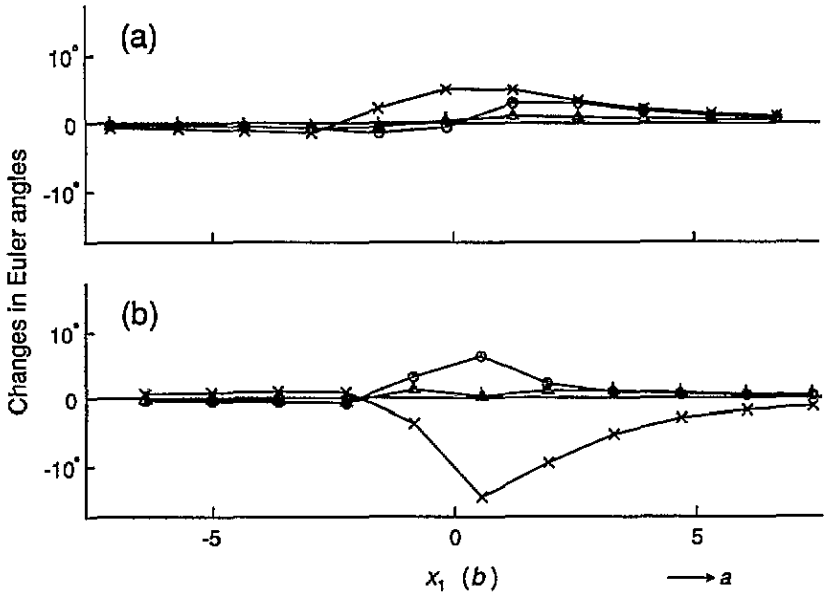

Figure 3. Orientational aspects of molecules around the dislocation. (*a*) Changes in Euler angles of the corner molecules in the *ab* plane just above the slip plane and (*b*) those of the centre molecules. Circles, triangles and crosses denote Euler angles θ, ϕ and ψ, respectively.

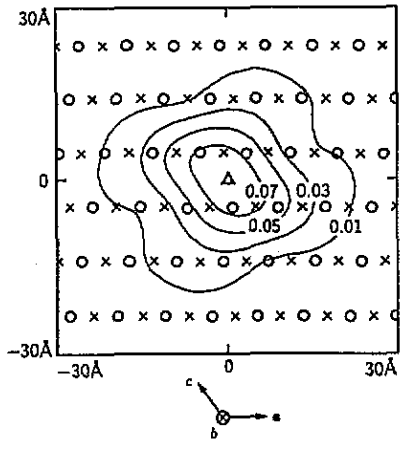

Figure 4. Equipotential curves ΔE (in eV): ΔE is the packing energy per unit lattice cell relative to that of a perfect crystal. A triangle denotes the dislocation centre, crosses the corner molecules, circles the centre molecules.

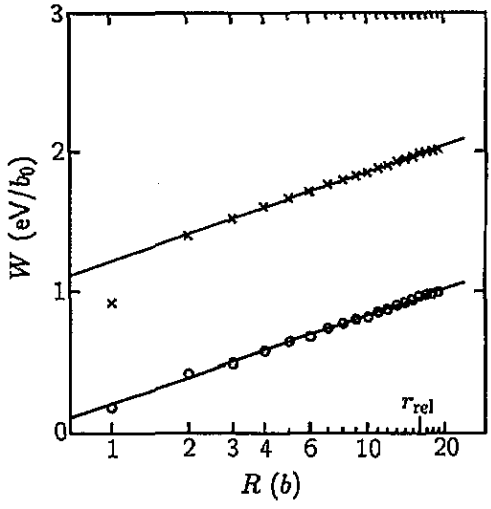

Figure 5. The strain energies per unit length, W, stored within a cylindrical region of radius R with its centre at the dislocation line. The abscissa is on a logarithmic scale. Crosses denote the energies before relaxation and circles those after relaxation.

The strain energies per unit length, W, stored within a cylindrical region of radius R, against ln R, are shown in figure 5 for the configurations before and after the relaxation. The pre-logarithmic energy factor after the relaxation is $0.27\,\mathrm{eV}/b_0$ ($7.32 \times 10^{-11}\,\mathrm{J\,m^{-1}}$), which

agrees very well with that estimated from anisotropic elasticity, and is smaller than that of the edge dislocation, $0.57\,\mathrm{eV}/a_0$ ($1.12 \times 10^{-10}\,\mathrm{J\,m^{-1}}$), where a_0 and b_0 are the lengths of the unit lattice vectors a_0 and b_0, respectively. The core energy within a cylindrical region of radius $5b$ is $0.64\,\mathrm{eV}/b_0$ ($1.74 \times 10^{-10}\,\mathrm{J\,m^{-1}}$), which is smaller than that of the edge dislocation, $1.28\,\mathrm{eV}/a_0$ ($2.51 \times 10^{-10}\,\mathrm{J\,m^{-1}}$). This shows clearly that the energy of the screw dislocation is lower than that of the edge dislocation.

3. Peierls stress for [010](001) dislocations

To identify the dislocations which control the slip deformations in (001)[010] systems, the Peierls stresses are calculated not only for the screw dislocation but also for the edge dislocation.

3.1. Method

The model crystal is the same as that used for the determination of the structure of dislocations. The Peierls stress is obtained using the following iterative procedures.

The stable molecular configuration around a dislocation under no external stress (i.e. $\sigma_{ex} = 0$), such as obtained in the previous section, is taken as the initial state. The external stress is increased by $\Delta\sigma_{ex}$ at the beginning of each step. In the present slip system, the slip plane is normal to the x_3 axis, and the Burgers vector $\boldsymbol{b}$ is parallel to the x_2 axis, so the most effective component of the stress to move dislocations would be σ_{23}. Hence the shear stress σ_{23} is applied to the crystal as the external stress σ_{ex}. In the present calculation, the values of the increment in stress are $2 \times 10^{-4}\ \mu$ and $1 \times 10^{-2}\ \mu$ for the edge and the screw dislocation, respectively, where μ is the shear modulus obtained from the energy factor of the screw dislocations; $\mu = (c_{44}c_{66} - c_{46}^2)^{1/2} = 2.65\,\mathrm{GPa}$. All the molecules in the crystal are translated and rotated in proportion to the strain corresponding to the increased stress.

Since the molecular configuration obtained above is not in equilibrium, the relaxations are repeated until a convergence condition is fulfilled; the convergence condition is mentioned in detail in the following subsection. We employed only the Newton method with the line search as the relaxation method.

After the relaxation the position of a dislocation is examined; the coordinates of the position are defined as

$$y_d = \int x_2\rho_2(x_2)\mathrm{d}x_2\left(\int \rho_2(x_2)\mathrm{d}x_2\right)^{-1} \qquad x_d = \int x_1\rho_2(x_1)\mathrm{d}x_1\left(\int \rho_2(x_1)\mathrm{d}x_1\right)^{-1}$$

for the edge and the screw dislocation, respectively, where ρ_2 is the x_2 component of the Burgers vector density (Víteck *et al* 1971). If the position after the relaxation moves over more than one lattice repeat distance along the slip plane from its initial position, the external stress at that step is regarded as an apparent Peierls stress τ_a. A Peierls stress τ_P is estimated using several values of the apparent Peierls stresses obtained under different conditions.

3.2. Convergence condition of relaxations

If any component of the displacement vectors of relaxable molecules during one relaxation step becomes less than a certain value δ, the molecules are regarded as relaxed and the relaxations under that stress are terminated (Minami *et al* 1974). The magnitude of the convergence criterion affects the results significantly. The dependence of the apparent

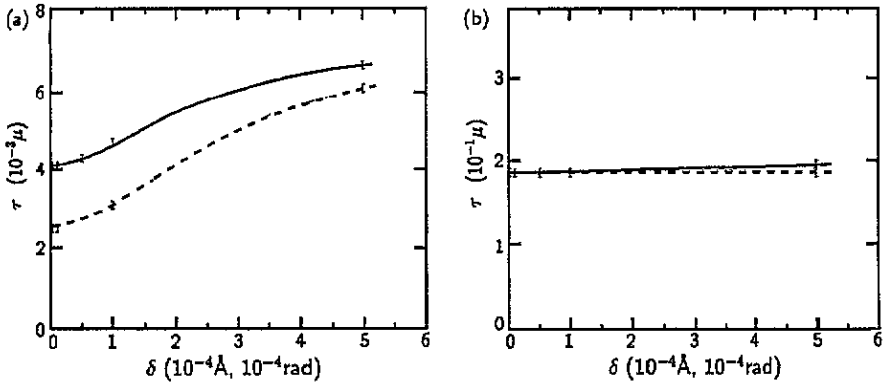

Figure 6. The dependence on the convergence criterion of the apparent Peierls stress of the edge dislocation (*a*), and of that of the screw dislocation (*b*). In both figures, full curves denote the dependence in the crystal with $r_{rel} = 6b$, and broken curves in that with $r_{rel} = 8b$.

Peierls stress τ_a on the value δ is shown in figure 6. The extrapolation to the ordinate gives the true value of the apparent Peierls stress in that model size. In the case of the edge dislocation, the apparent Peierls stress was affected strongly by the magnitude of δ. The ratios of the apparent Peierls stress for $\delta = 5 \times 10^{-4}$ to that for $\delta = 1 \times 10^{-6}$ are 1.6 and 2.4 for $r_{rel} = 6b$ and $8b$, respectively: the units of δ are Å or radians, and for the purposes of abbreviation are omitted below. Since the same value of the apparent Peierls stress was obtained for $\delta = 1 \times 10^{-5}$ to 1×10^{-6} in both cases of $r_{rel} = 6b$ and $8b$, it should be sufficient to adopt $\delta = 1 \times 10^{-5}$ as the convergence criterion for the calculation on the edge dislocation. On the other hand, in the case of the screw dislocation, the apparent Peierls stress is hardly affected by the magnitude of δ. The apparent Peierls stress becomes the same value for $\delta < 1 \times 10^{-4}$ ($r_{rel} = 6b$) and $\delta < 5 \times 10^{-4}$ ($8b$), so that we also adopt 1×10^{-5} for the calculation of the screw dislocation. All the results shown below were obtained using $\delta = 1 \times 10^{-5}$.

3.3. Results

Figure 7 shows the positions of the edge dislocation, y_d, against the external stress, σ_{ex}, for three relaxation radii. In the smaller models the dislocation stops several times before its motion reaches one lattice repeat distance, as shown in figure 7(*a*) and (*b*). This arises from the fact that the edge dislocation has a shear misfit region spreading along the slip plane, in which the non-elastic displacements of molecules corresponding to the small motion of the dislocation take place by increasing external stress. The effective stress acting on the dislocation is relaxed partly even by the small motion, due to the existence of the fixed region. For this reason, as the model size increases, the dislocation starts to move through fewer small motions, and finally moves through one motion, as shown in figure 7(*c*). Hereinafter, the stress at which the dislocation begins to move and that at which the motion reaches one lattice repeat distance will be referred to as τ_i and τ_f, respectively. Since in the computation of the Burgers vector density $\rho_2(x_2)$ the abscissa is taken as the x_2 coordinate of the molecules in the compression region, the value of y_d at τ_f does not reach exactly one in the figure; the magnitude of the strain in the compression region in the core is almost the same over $5b$ along the slip plane, and is about 0.05 for $r_{rel} = 16b$.

Figure 8 shows the positions of the screw dislocation, x_d, against the external stress, σ_{ex}. In the case of the screw dislocation, the dislocation moves over more than one lattice repeat

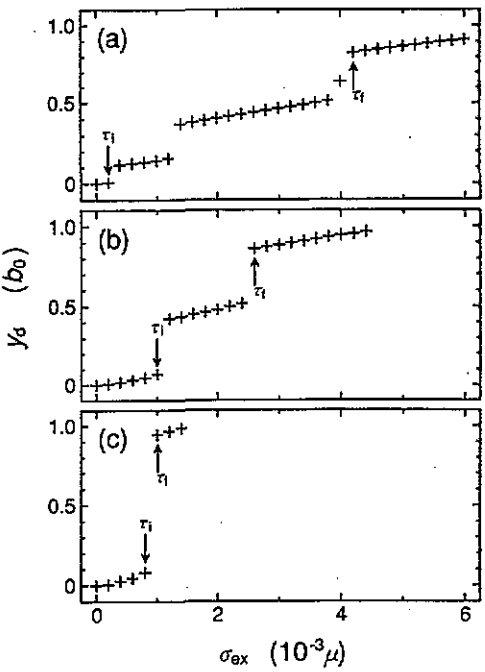

Figure 7. The positions y_d of the edge dislocation along the slip plane against the external stress σ_{ex}. (*a*) $r_{rel} = 6b$, (*b*) $r_{rel} = 8b$ and (*c*) $r_{rel} = 16b$.

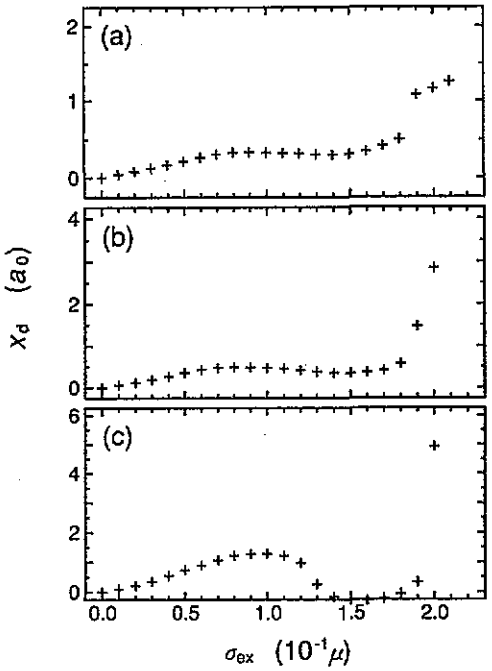

Figure 8. The positions x_d of the screw dislocation along the slip plane against the external stress σ_{ex}. (*a*) $r_{rel} = 6b$, (*b*) $r_{rel} = 8b$ and (*c*) $r_{rel} = 16b$.

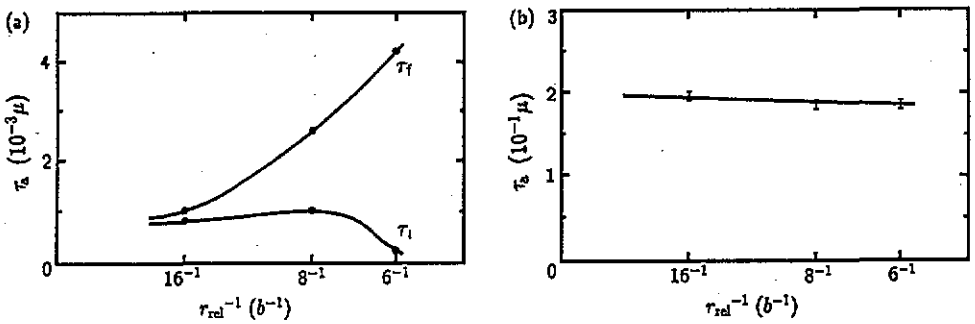

Figure 9. The dependence of the apparent Peierls stress on the model size. The abscissa indicates the inverse of the model size, r_{rel}^{-1}. The extrapolated value to the ordinate shows the true Peierls stress τ_P in the present model. (*a*) The edge dislocation. (*b*) The screw dislocation.

distance through one motion, because the strain caused by the screw dislocation concentrates into a relatively narrow region, and the magnitude of the external stress is very large in comparison with the case of the edge dislocation. The curves of the positions x_d wind, particularly in figure (*c*), because the distribution of the Burgers vector is greatly disturbed due to the large external stress. From the position of the peak of the distribution, however, the stress at which the dislocation begins to move plastically is easily distinguished.

Figure 9 shows the effect of the relaxation radius on the apparent Peierls stress. The extrapolation of the apparent Peierls stress to an infinitely large model gives a true Peierls

stress τ_P in the present simulation. In the case of the edge dislocation, the value of τ_f decreases as the relaxation radius r_{rel} increases, but that of τ_i almost saturates for models larger than $r_{rel} = 8b$. Thus the true Peierls stress τ_P(edge) is regarded as $0.8–1.0\times10^{-3}$ μ. On the other hand, for the screw dislocation, the values of τ_a are little affected by the model size. The true Peierls stress τ_P(screw) is regarded as $1.9–2.0\times10^{-1}$ μ. Judging from the magnitude of these two Peierls stresses, it is the screw dislocations that control the plastic deformations in the present slip system of anthracene crystals at low temperature.

4. Discussion

It was found that the distribution of the shear strain $\varepsilon_{2\theta}$ around the screw dislocation was strongly anisotropic and the molecular configurations had a complete twofold symmetry with respect to the dislocation centre. Its core region did not spread as much as that of the edge dislocation. The shear strain, chief in the screw dislocation, could become large near the dislocation centre, since rotations of molecules around those normal axes were easily caused at low energy and contributed to that strain. The energy of the screw dislocation was lower than that of the edge dislocation.

It was also found from the present simulation that the value of the Peierls stress of the screw dislocation was much larger than that of the edge dislocation. This is consistent with the relation of the core widths of dislocations, i.e. that the core width of the screw dislocation is narrower than that of the edge dislocation. The anthracene crystals are brittle below about 100 K, and fracture by external stress without plastic deformation. The extrapolation of yield stress to 0 K using the experimental values at the temperature from 110–150 K gives 4.6×10^{-3} μ (Kojima and Okada 1990). This value is between the calculated Peierls stress of the edge dislocation and that of the screw dislocation, but the latter is considerably higher.

The elastic constants calculated in the present model were compared with the experimental ones to check the reliability and the limitations of the model. The former are rather larger than the latter, as seen in table 1. We also used all the other potential parameter sets cited by Pertsin and Kitaigorodsky (1987) to evaluate the elastic constants, but the differences between the calculated and the experimental values were of the same order. One of the reasons for these discrepancies arises from the difference in temperatures at which the elastic constants were evaluated. Although a few components have opposite signs among three sets of the elastic constants listed in table 1, the components that are significant to the formation and motion of the screw dislocation, i.e. c_{44}, c_{66} and c_{46}, are in comparatively good agreement. Hence the difference between the calculated and the experimental values of the elastic constants do not lead to the large discrepancy between the Peierls stress in the present model and the yield stress extrapolated to 0 K in the experiments.

To investigate the causes of the high Peierls stress of the screw dislocation, we evaluated the shape of the Peierls potential (Ide *et al* 1992). However, only in the range $(\frac{3}{4} \pm 0.114)a_0 + \frac{1}{2}c_0$ in figure 1 could the potential curve be obtained, and there was no section at which the gradient was so steep that the Peierls stress became large. From the behaviour of the screw dislocation under the external stress, it may be considered that there exists a section with a steep gradient corresponding to a high Peierls stress outside the range evaluated.

To confirm that the high Peierls stress was caused not by an undesirable behaviour in numerical treatments (such as falling into a local minimum), but by the characteristic features in the crystals composed of large molecules, we also performed the molecular dynamics at

finite temperature, in which the potential barrier between a local minimum and the absolute minimum can be overridden, owing to the kinetic energy. The model crystal was the same as that used in the static method, and only the molecules in the inner region could move under the condition that the temperature and the strain applied to the outer fixed region were kept constant. The periodic boundary condition used above was also used in this case, so that kinks were not taken into account; this calculation using molecular dynamics was made not to reproduce actual phenomena, but to confirm the result obtained by the static method. It was found from the molecular dynamics that the external shear stress required to move the dislocation had a strong dependence on temperature (Ide *et al* 1992). The stress at 20 K was half that at 0 K. The stress interpolated at 110 K was about $1 \times 10^{-2}\ \mu$, while the experimental yield stress at 110 K was $1.4 \times 10^{-3}\ \mu$ (Kojima and Okada 1990). This discrepancy arises from the lack of kinks in the present model. The dislocation could then move freely above 160 K without the external stress in our model. Thus the stress required to move the screw dislocation decreased continuously as the temperature increased, and the value of the stress at 0 K was not so high judging from those at low temperatures. This suggests that the yield stress of anthracene crystals, composed of disk-like molecules, may also depend strongly on the temperature at low temperatures.

The results for the screw dislocation obtained in the present calculations have several similarities to a $\frac{1}{2}a\langle 111\rangle$ screw dislocation in BCC crystals; the strongly anisotropic strain field, the extension of the strain field out of the slip plane on which the dislocation moves, the high Peierls stress, the strong dependence of the mobility of the dislocation on temperature, and so on.

One of the reasons for the high Peierls stress of the screw dislocation is that the molecular configuration around molecule E in figure 2 is hard to alter through the external shear stress σ_{23}. In particular, the relative displacement of molecule E to neighbouring molecules in the b direction, which is significant to the movement of the screw dislocation, cannot become large. Corresponding to this, the forces on molecule E become large compared with those on the others, as the external stress increases; the force acting on an atom in molecule E at $\sigma_{ex} = 1.9 \times 10^{-1}\ \mu$ is about three times the value of that in a perfect crystal. Thus, the characteristic molecular configuration around the dislocation, which reflects the peculiar shape of the molecules, results in a large Peierls stress in molecular crystals, although a low Peierls stress may be expected because of the weak van der Waals intermolecular interaction.

The Peierls stress obtained through the present model may be lowered if something that can change the molecular configuration around E, such as the deformation of molecules and the effect of the stress component except σ_{23} and so on, is taken into account. However, the value of the Peierls stress of the screw dislocation is not greatly lowered in comparison with the core widths of the screw and the edge dislocation. Thus, it seems certain that the plastic deformation is controlled by the screw dislocations in the present slip system at low temperatures.

Acknowledgments

We would like to thank the staff of the Computer Centre of Yokohama City University for useful advice. The numerical calculations were partially carried out at the Computer Centre of University of Tokyo. This work was supported in part by a Grant-in-Aid for Scientific Research from the Ministry of Education, Science and Culture, Japan and also by a Grant-in-Aid from Yokohama City.

References

Afanas'eva G K and Miasnikova R M 1970 *Kristallografiya* **15** 189
Bacon D J and Tharmalingam K 1983 *J. Mat. Sci.* **18** 884
Chaplot S L, Lehner N and Pawley G S 1982 *Acta Cryst.* B **38** 483
Cohen M D, Ludmer Z, Thomas J M and Williams J O 1969 *Chem. Commun.* 1172
Craig D P and Markey B R 1979 *Chem. Phys. Lett.* **62** 223
Danno T and Inokuchi H 1968 *Bull. Chem. Soc. Japan* **41** 1783
Dautant A and Bonpunt L 1986 *Mol. Cryst. Liq. Cryst.* **137** 221
Gibson J B, Goland A N, Milgram M and Vineyard G H 1960 *Phys. Rev.* **120** 1229
Hirth J P and Lothe J 1982 *Theory of Dislocations* 2nd edn (New York: Wiley) p 436
Ide N, Okada I and Kojima K 1990 *J. Phys.: Condens. Matter* **2** 5489
—— 1992 *Trans. Mat. Res. Soc. Japan* **9** 98
Kojima K 1979 *Phys. Status Solidi* a **51** 71
—— 1987 *J. Appl. Phys.* **62** 1368
Kojima K and Okada I 1990 *Phil. Mag.* A **61** 607
Minami F, Kuramoto E and Takeuchi S 1974 *Phys. Status Solidi* a **22** 81
Mokichev N N and Pakhomov L G 1982 *Sov. Phys.–Solid State* **24** 1925
Okada I, Sugawara M and Kojima K 1989 *J. Phys.: Condens. Matter* **1** 3555
Pertsin A J and Kitaigorodsky A I 1987 *The Atom–Atom Potential Method* (Berlin: Springer) p 69
Robinson P M and Scott H G 1967 *Acta Metall.* **15** 1581
Silinsh E A 1980 *Organic Molecular Crystals* (Berlin: Springer) p 5
Víteck V, Lejček L and Bowen D K 1971 *Interatomic Potentials and Simulation of Lattice Defects* ed P C Gehlen *et al* (New York: Plenum)
Williams D E 1966 *J. Chem. Phys.* **45** 3770
Williams J O and Thomas J M 1972 *Mol. Cryst. Liq. Cryst.* **16** 371